TABLE OF CONTENTS (TOC)

Water-soluble hollow nanocrystals from self-assembly of AIEE-active Pt(II) metallomesogens

Cristián Cuerva,[a] * Javier Fernández-Lodeiro,[a,b] Mercedes Cano,[c] José Luis Capelo-Martínez,[a,b] Carlos Lodeiro[a,b] *

[a] BIOSCOPE Research Group, LAQV@REQUIMTE Chemistry Department, NOVA School of Science and Technology, NOVA University Lisbon, 2829-516 Caparica (Portugal). E-mail: c.alaiz@fct.unl.pt; cle@fct.unl.pt

[b] PROTEOMASS Scientific Society, Rua dos Inventores, Madam Parque, Caparica Campus, 2829-516 Caparica (Portugal). E-mail: clodeiro@bioscopegroup.org

[c] Department of Inorganic Chemistry, Complutense University of Madrid, Ciudad Universitaria, 28040 Madrid (Spain).

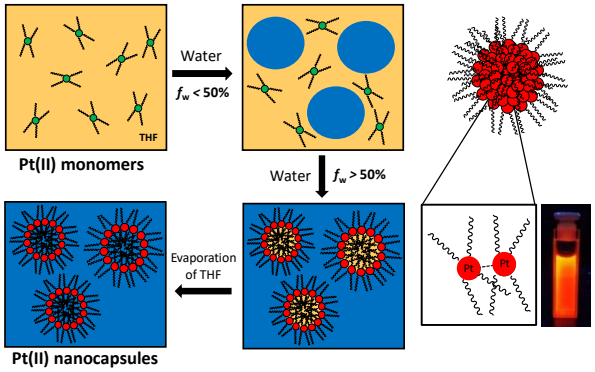

We have demonstrated that luminescent Pt(II) metallomesogens can be well-dispersed in water despite their great hydrophobic nature, forming nanocapsules useful for entrapment of hydrophobic drugs.

Provide the authors' webside if possible.

C. Cuerva, J. Fernández-Lodeiro, J. L. Capelo-Martínez, C. Lodeiro – https://www.bioscopegroup.org

M. Cano, https://www.ucm.es/matmopol

Nano Research
DOI (automatically inserted by the publisher)
Research Article
ISSN 1998-0124
CN 11-5974/O4

Water-soluble hollow nanocrystals from self-assembly of AIEE-active Pt(II) metallomesogens

Cristián Cuerva[1] (✉), Javier Fernández-Lodeiro[1,2], Mercedes Cano[3], José Luis Capelo-Martínez[1,2] Carlos Lodeiro[1,2] (✉)

[1] *BIOSCOPE Research Group, LAQV@REQUIMTE Chemistry Department, NOVA School of Science and Technology, NOVA University Lisbon, 2829-516 Caparica (Portugal). E-mail: c.alaiz@fct.unl.pt; cle@fct.unl.pt*
[2] *PROTEOMASS Scientific Society, Rua dos Inventores, Madam Parque, Caparica Campus, 2829-516 Caparica (Portugal). E-mail: clodeiro@bioscopegroup.org*
[3] *Department of Inorganic Chemistry, Complutense University of Madrid, Ciudad Universitaria, 28040 Madrid (Spain).*

† In loving memory of Professor José A. Campo Santillana

Received: day month year
Revised: day month year
Accepted: day month year (automatically inserted by the publisher)

KEYWORDS

Pt(II) metallomesogens; self-assembly; luminescent nanomaterials; droplets; nanocapsules.

ABSTRACT

Luminescent hollow micro- and nanocrystals have been successfully obtained taking advantage of the self-assembly behavior and the aggregation-induced emission enhancement properties of several bispyrazolate Pt(II) metallomesogens decorated with four terminal alkyl chains. Oil-in-water droplets have been used to confine the Pt(II) compounds and drive them to be self-assembled *via* intermolecular Pt···Pt interactions into spherical aggregates of about 200 or 50 nm. Evaporation of the oil phase generates highly-stable aqueous dispersions of nanocrystals that emit a bright orange light as a result of the existence of ^{3}MMLCT excited states. Different methods and conditions have been tested for studying the effect of several parameters such as the temperature and the stirring speed in the final particle size and in the polydispersity index. Moreover, the micro- and nanocrystals are able to entrap hydrophobic drugs between the alkyl chains of the compounds, forming stable dispersions of drug-loaded capsules in water. The droplet method is applied in the area of metallomesogens for the first time to synthesize self-assembled Pt(II) nanocapsules, which opens a new field of study that could allow the use of these liquid crystal materials in biomedical applications.

1 Introduction

Molecular self-assembly is a powerful tool to enhance the luminescence properties of a dye purely organic or a coordination compound. It is well-known that aggregation can be one of the main complications when a luminescent probe has to be used in solution at high concentrations or in the solid state. Aggregation-caused quenching (ACQ) effect constitutes a vital drawback for designing

Address correspondence to Cristián Cuerva, c.alaiz@fct.unl.pt; Carlos Lodeiro, cle.fct.unl.pt

highly-efficiency luminescent materials [1]. A significant number of organic compounds and complexes have been described to exhibit high fluorescence quantum yields in dilute solutions but, in the solid state, they hardly emit light [2-4]. Fortunately, there are some strategies to mitigate this effect [5-7]. With the increase of concentration, molecules also have a great ability to establish short contacts and, in such conditions, intermolecular interactions play a key role. The self-assembly of π-extended compounds favors the restriction of intramolecular rotation, and this can cause an aggregation-induced emission enhancement (AIEE) as a result of the activation of new radiative transitions [8]. This behavior was discovered for the first time in 2001 and, since then, a large library of AIEE organic compounds and metal complexes have been reported in the literature [9-17].

In particular, the self-assembly behavior of Pt(II) compounds has attracted special attention because of their interesting photophysical properties. As a consequence of the strong spin-orbit coupling induced by the metal center, the Pt(II) complexes can behave as phosphorescent materials at room temperature [18-20]. Moreover, they can also exhibit chromic properties upon coordination to adequate ligands. In the monomer form, the photophysical properties are mainly dominated by intraligand (IL) or metal-to-ligand (ML) charge transfers, which usually results in a greenish-yellow emission. Otherwise, aggregation *via* intermolecular Pt···Pt interactions originates triplet metal-metal-to-ligand charge transfer (^{3}MMLCT) excited states, causing a remarkable red-shift of the emission band [21,22]. Thus, by controlling the supramolecular assembly of these systems, it is possible to control their photophysical properties and to create smart materials that combine chromic and AIEE behaviors for real application in fields such as security and energy, or even biomedicine [23-26].

In this respect, we have recently synthesized several families of discotic pyridine- and isoquinoline-functionalized bispyrazolate Pt(II) metallomesogens which are able to self-assembly into columns *via* intermolecular π···π and Pt···Pt interactions [27-29]. Although restriction of intramolecular rotations is produced, the presence of alkyl chains contributes to increasing the flexibility of the molecules and, as a consequence, the compounds exhibit mesomorphism in surprisingly wide temperature ranges of up to 300 ºC. The molecular assembly concomitantly originates ^{3}MMLCT excited states that result in a color change from greenish to bright orange. Nevertheless, not only temperature causes the formation of these aggregates, pressure or rubbing can also induce the establishment of these Pt···Pt contacts [28,29]. This self-assembly behavior is reversible, so that the exposure of the compounds to certain solvents or vapors breaks the Pt···Pt interactions and the initial greenish emission can be recovered.

In our previous works, we demonstrate that Pt(II) metallomesogens can be excellent candidates to fabricate stimuli-responsive thin films for sensor applications [30]. Herein, we explore the self-assembly behavior and AIEE properties of several bispyrazolate Pt(II) metallomesogens in aqueous solutions (Scheme 1). Even though none of these compounds are soluble in water, they have an amphiphilic character that has allowed achieving the self-assembly of molecules into micellar-like aggregates, giving rise to highly stable dispersions of luminescent micro- and nanocrystals in aqueous media.

2 Experimental

2.1 Materials

The pyridine- and isoquinoline-functionalized bispyrazolate Pt(II) compounds **1** – **6** were synthesized as we described previously [27-29]. Coumarin-6 (C6) was purchased from Sigma-Aldrich. Solvents were purchased from PanReac and used without further purification. Ultrapure deionized water was used in all the experiments.

2.2 Synthesis of micro- and nanocrystals from 2

Method 1. To a solution of **2** (0.5 mg) in 2.6 mL of THF were slowly added 0.4 mL of deionized water in a vial with a section of 22 mm. Oil-in-water (O/W) droplets containing the self-assembled Pt(II) compound were formed under magnetic stirring at 300 rpm during 5 min. The mixture was then storage at 20 ºC (or 4 ºC) in the absence of light for 24 h to

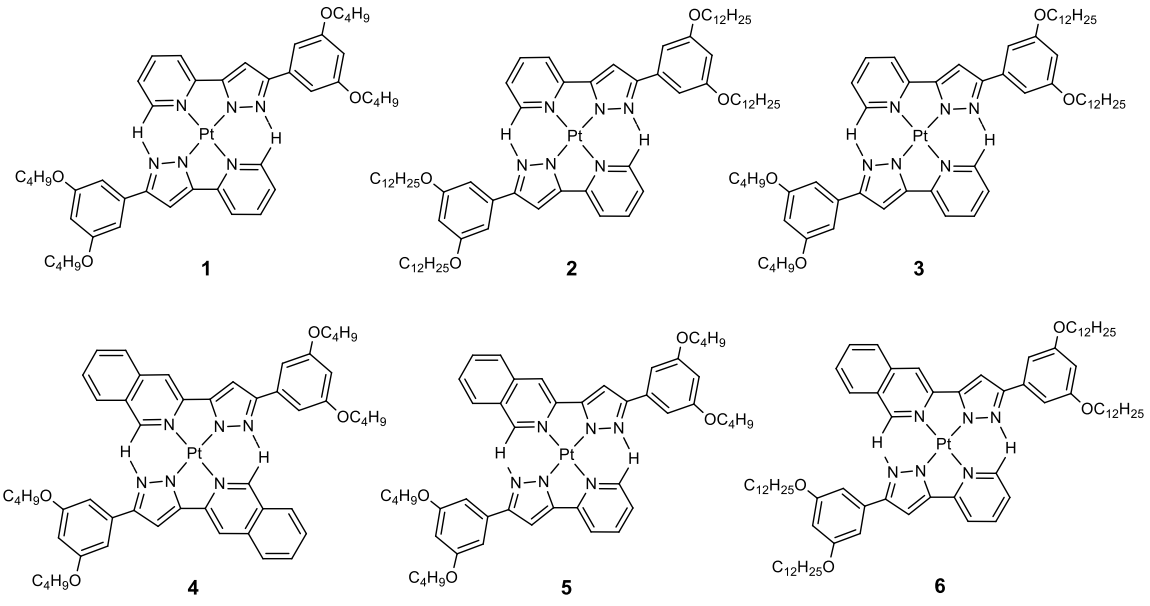

Scheme 1 Molecular structure of the Pt(II) metallomesogens used in the fabrication of luminescent O/W droplets

stabilize the droplets. THF was removed by slow evaporation at room temperature for 24 h without stirring, giving rise to the colloidal dispersions of the corresponding micro- or nanocrystals. Aqueous solutions were filtered using glass membranes with a pore size of 10 – 15 μm to remove any precipitate of the Pt(II) compound before use.

Method 2. Microcrystals of **2** were prepared as method 1 but adding quickly the solution of **2** over the deionized water under magnetic stirring at 300 rpm during 5 min., and stabilizing the droplets at 20 ºC for 24 h without stirring.

2.3 Synthesis of micro and nanocrystals from 5

Micro- and nanocrystals of **5** were prepared as those of **2** following method 1. To a solution of **5** (0.3 mg) in 2.6 mL of THF were slowly added 0.4 mL of deionized water under magnetic stirring at 300 rpm, stabilizing the O/W droplets at 20 ºC (or 4ºC) for 24 h. The reaction vessel used was a vial with a section of 22 mm. Evaporation of THF at room temperature during 24 h gave to aqueous dispersions of the corresponding micro- or nanocrystals of **5**, which were filtered using glass membranes (porosity: 10 – 15 μm) in order to remove any remainder of **5** that had not been well-assembled.

2.4 Synthesis of C6-loaded microcapsules

C6-loaded micro- and nanocapsules of **2** and **5** were obtained through the droplet method as follows. Firstly, a solution containing 1.70 mg of C6 was prepared in 10 mL of THF. Another solution was then prepared from an aliquot of 0.6 mL of the C6 solution, and 0.5 mg of **2** (or 0.3 mg of **5**). The mixture was quickly added over 2.6 mL of water in a vial with a section of 22 mm, maintained mechanical stirring at 300 rpm during 5 min. The solution was storage at 20 ºC (or 4 ºC) in the absence of light for 24 h to stabilize the self-assembly of the Pt(II) compound and the entrapment of C6 in the O/W droplets. After this period, THF was eliminated by slow evaporation at room temperature for 24 h. Aqueous solutions containing the C6-loaded capsules were filtered through glass membranes with a pore size of 10 – 15 μm to remove any precipitate before use.

2.5 Methods

2.5.1 DLS Measurements

Dynamic light scattering (DLS) were performed by using a Malvern Zetasizer Nano series (Worcestershire, WR14 1XZ, UK) from PROTEOMASS Scientific Society-BIOSCOPE Facility Lab. Samples were analyzed by using glass cells at a

scattering angle of 90º and at temperature of 20 ºC. A dip cell is used for the measurement of the ζ-potential of micro and nanocrystals. For temperature-dependent studies, samples were stabilized for 5 minutes before performing measurements.

2.5.2 TEM analysis

Transmission electron microscopy (TEM) images were obtained using a JEOL JEM 1010 transmission electron microscope from the CACTI, University of Vigo (Spain), operating at 100 kV. Samples were prepared dropping 5 μL of the colloidal suspension on a copper grid coated with a continuous carbon film, and the solvent was allowed to evaporate. Size of particles and histograms were calculated from TEM images using the ImageJ software (Image 1.51 h, Wayne Rasband, National Institutes of Health, Bethesda, MD, USA).

2.5.3 Powder XRD analysis

Powder X-ray diffraction analysis was carried out on a Panalytical X'Pert PRO MPD diffractometer with Cu-Kα (1.54 Å) radiation in a θ–θ configuration (X-Ray Diffraction Service of the Complutense University of Madrid (Spain)). Sample was prepared dropping 2 mL of the colloidal suspension of microcrystals of **2** on a silicon support, and the solvent was allowed to evaporate at room temperature.

2.5.4 Photophysical measurements

UV-Vis absorption spectra were recorded on a Jasco V-650 spectrophotometer, and the emission and excitation spectra by using a Horiba-Jobin-Yvon Fluoromax-4 spectrofluorimeter in the PROTEOMASS-BIOSCOPE facilities. The stock solutions for the photophysical characterization of the Pt(II) compounds in tetrahydrofuran (*ca.* 10^{-3} M) were prepared by dissolving an appropriate amount of the corresponding compound in a 10 mL volumetric flask and diluting to the mark with tetrahydrofuran. The studied solutions were prepared by appropriate dilution of the stock solutions up to 10^{-5}-10^{-6} M. All measurements were performed at 298 K (λ_{exc} = 345 nm). The absolute photoluminescence quantum yields of the Pt(II) aggregates in the colloidal suspensions were recorded with an integrating sphere accessory for a Horiba Jobin-Ybon SPEX Fluorolog 3.22 spectrofluorimeter. All the measurements were performed under an air atmosphere.

2.5.5 Encapsulation efficiency and loading capacity

Encapsulation efficiency was estimated through quantitative determination of the amount of non-entrapped C6 by UV-Vis spectroscopy. Samples were obtained by successive extractions of the aqueous dispersions containing the C6-loaded capsules with chloroform (3 x 1 mL). Since the organic phase could contain both non-entrapped C6 and monomers of the Pt(II) compound, chloroform was eliminated in vacuum and then, 3 mL of ethanol were added to solve C6. The solution was filtered in vacuum prior to UV-Vis measurements. The calibration curve of C6 in ethanol was obtained at 458 nm in the range of 0.76 – 1.90 μg/mL. The encapsulation efficiency (EE) and the loading capacity (LC) were calculated as follows:

$$E(\%) = \frac{W_{total} - W_{free}}{W_{total}} \text{ x } 100 \quad (1)$$

$$LC(\%) = \frac{W_{entrapped}}{W_{entrapped} + W_{capsules}} \text{ x } 100 \quad (2)$$

where W_{total} is the starting amount of C6 used; W_{free} is the amount of non-entrapped C6 calculated by UV-Vis spectroscopy; $W_{entrapped}$ is the amount of C6 entrapped inside the capsules; and $W_{capsules}$ is the starting amount of the Pt(II) compound.

3 Result and discussion

3.1 Self-assembly and AIEE properties

The excitation and emission spectra of the Pt(II) compounds **1**-**6** in THF solution (1.0 x 10^{-5} M) are depicted in Figure 1. It is observed two excitation bands at around 360 and 435 nm, which can be attributed to singlet metal-to-ligand charge transfers

(1MLCT), and metal-metal-to-ligand charge transfers (MMLCT) in both singlet and triplet excited states, respectively [31]. All the emission spectra show similar profiles, with bands centered at *ca.* 500 – 570 nm that are originated from 1MLCT in monomeric species.

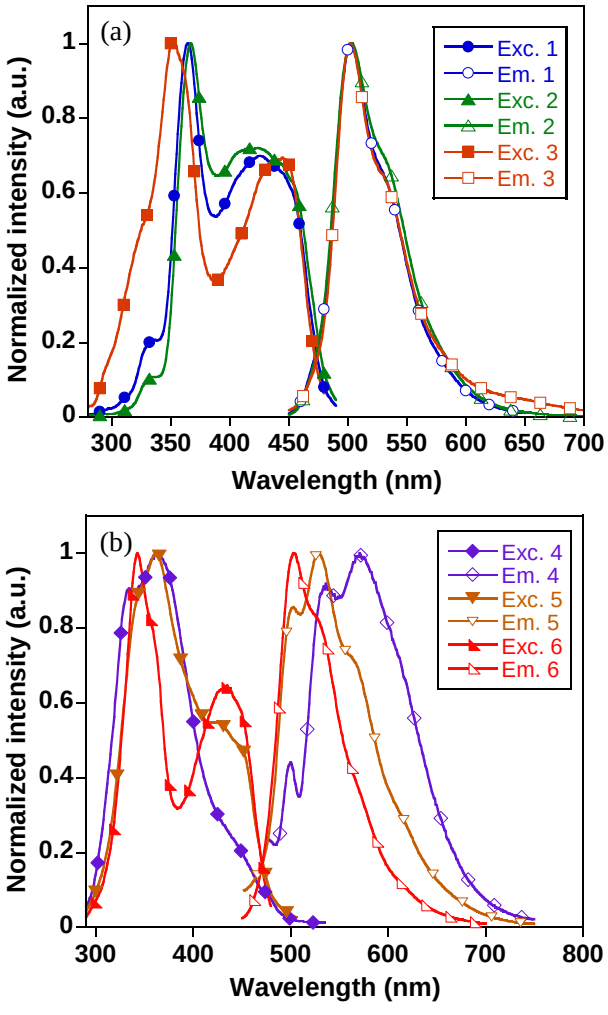

Figure 1 Excitation and emission spectra of the Pt(II) compounds **1**-**6** in THF solution (1.0 x 10^{-5} M).

As we previously reported, these compounds exhibit a great ability to form aggregates *via* permutable Pt···Pt intermolecular interactions in the solid state [28,29]. Thus, we were interested in studying their luminescence behavior at high concentrations. As shown in Figure S1 in the ESM for **2**, the emission band remains centered at 500 nm, and only an increase in its intensity is observed by increasing the concentration of the Pt(II) compound. This fact indicates that aggregation does not occur, and molecules are maintained in the monomeric form.

Since THF is water-miscible and the Pt(II) compounds are not soluble in water, mixtures of both solvents could cause a confinement of the molecules, restricting their mobility and favoring the formation of aggregates. Figure 2(a) displays the emission spectra of **2** in THF/water mixtures with different water content. Note that at low water fractions (f_w) from 20 to 40 %, three new bands appear at 540, 567 and 605 nm, which is a clear indication of the existence of aggregates in solution. The first two emission bands can be associated with 1MLCT originated by the formation of aggregates through π···π interactions between the pyridine and/or the benzene groups of the pyrazolate ligands [32]. Meanwhile, the band located at 605 nm can be attributed to 3MMLCT as a result of the establishment of intermolecular Pt···Pt interactions [33]. Nonetheless, aggregation is not complete because the typical monomer emission continues to appear at 500 nm. Due to the solubility of **2** gradually decreases upon increasing the water content from 20 to 40%, it is not surprising that the compounds precipitate, as demonstrated in Figure 2(c). By contrast, in mixtures with high f_w from 50 to 90%, the emission intensity is enhanced by over 80% respect to the original one in pure THF (Φ = 0.1), and solid precipitates are not observed (Figure 2(a,c)). It should also be noted that the spectra display only the 3MMLCT band so that all the molecules are self-assembled into aggregates.

Similar features were found for the remaining Pt(II) compounds analyzed in this work, except for **4**, which precipitates after the addition of water (Figure S2(a-c) in the ESM). The AIEE effect is observed even for the unsymmetrical bis(pyridylisoquinolinylpyrazolate) derivatives **5** and **6** that practically do not emit in pure THF solution (Φ < 0.01) and show quantum yields of *ca.* 0.1 in the aggregated form (Figures 2(b,c) and S2(c) in the ESM).

For an in-depth understanding of the AIEE behavior of these systems, dynamic light scattering (DLS) experiments were performed in the THF/water

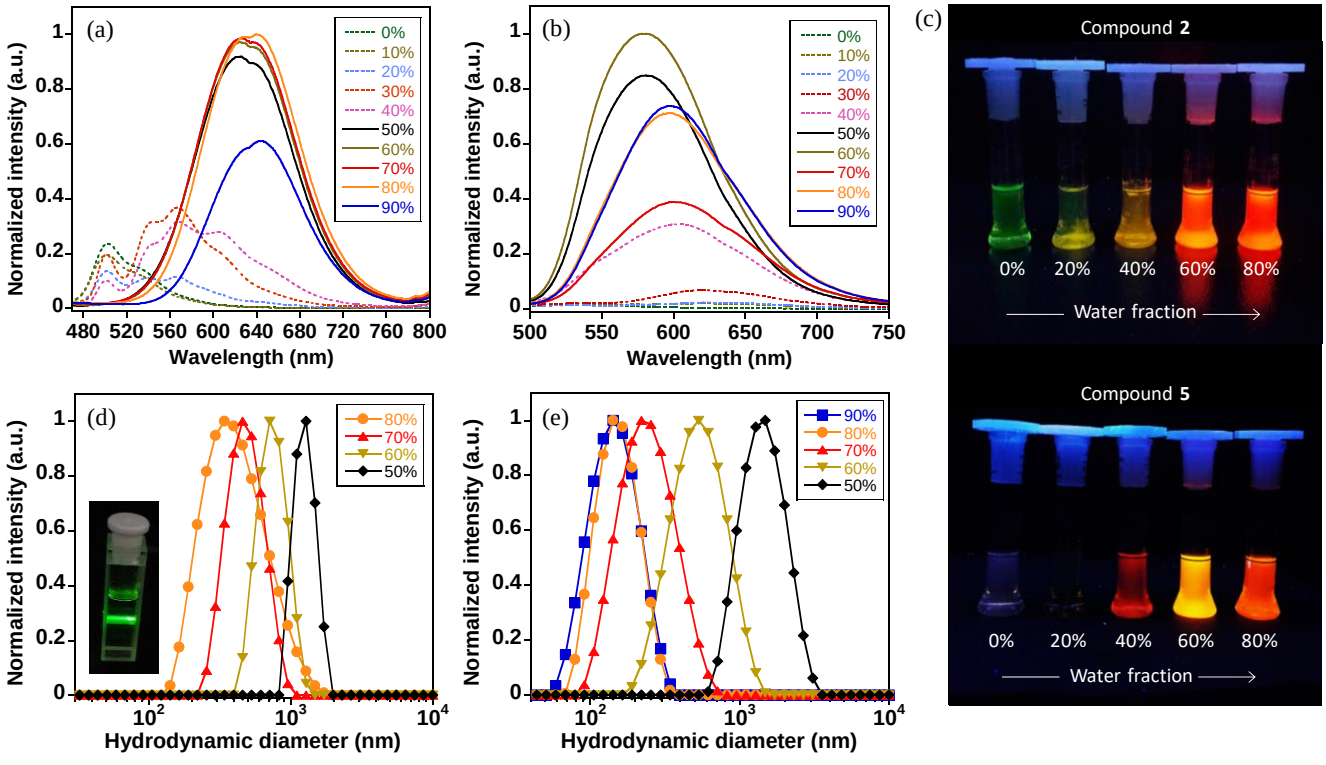

Figure 2 AIEE behavior of the Pt(II) compounds: (a,b) Normalized emission spectra for compounds **2** and **5**, respectively, in the THF/water mixtures as a function of the water fraction f_w. (c) Images of the THF/water mixtures taken under UV light (λ_{exc} = 365 nm). (d,e) Size distributions for the Pt(II) aggregates **2** and **5** as a function of the water fraction f_w, obtained from DLS analysis. The inset shows the Tyndall effect observed in the THF/water mixture of **2** with f_w = 80%.

mixtures. As expected, no evidences of a colloidal dispersion of aggregates were observed at low f_w between 10 and 40% (data not shown). However, DLS measurements confirmed the existence of well-dispersed microaggregates in the THF/water mixtures of **2** and **5** when $f_w \geq 50\%$ (Figure 2(d,e)). It is noteworthy that the addition of water causes a decreasing of the average hydrodynamic diameter of the aggregates, which reaches values of about 290 and 130 nm for **2** and **5**, respectively, with a polydispersity index (PDI) of 0.1-0.2. These results clearly reflect the space confinement to which the molecules are subjected. Thus, by increasing the water content above $f_w \geq 50\%$, oil-in-water (O/W) droplets containing the Pt(II) compounds are formed, and the AIEE effect is originated when the droplet diameter is so smaller than the mobility restrictions favor the formation of microaggregates through Pt···Pt interactions. The progress of this space confinement is clearly detected for compound **5**. Since its molecular structure has smaller alkyl chains than those of the analogous compounds, the solubility of **5** in THF is higher, so that the mobility restrictions when O/W droplets are formed at f_w = 50 - 60% are less. As a result, an AIEE effect is observed, but the emission maximum appears at *ca.* 580 nm (Figure 2(b,c)), which is in agreement with the formation of aggregates *via* interligand π···π interactions (average size: 1243 - 488 nm). The orange emission attributed to the Pt···Pt microaggregates is only observed when f_w is about 70 - 90% and therefore, the space confinement is rather high (average size: 223 - 130 nm).

Table S1 collects the average hydrodynamic diameter of the aggregates obtained from all the Pt(II) compounds, as well as the polydispersity index of the different colloidal dispersions. By comparing them, compounds **2** and **5** formed stable aggregates in several THF/water ratios from f_w = 50% to f_w = 90%, whereas high water contents were required to stabilize the aggregates of **1**, **3** and **6**. In particular, for **3**, the average diameter measured by DLS is *ca.* 1332

nm, which indicates that the introduction of asymmetry in the chain length does not favor the self-assembly of these systems. Likewise, the isoquinoline group seems to constitute a drawback to achieve the stabilization of the Pt···Pt aggregates because precipitation was observed for **4** in all the THF/water mixtures prepared. This effect is minimized in the unsymmetrical compounds **5** and **6**, in which one of the coordinated isoquinoliylpyrazolate ligands is substituted by a pyridylpyrazolate one. On the other hand, the alkyl chain length also has a certain influence on the size of these systems, obtaining smaller aggregates from compounds decorated with alkyl chains of four carbon atoms. Additional optical visualization and DLS experiments were also carried out to evaluate the stability of all dispersions for three months. Precipitation was observed in most cases along the first week, with the exception of the colloidal dispersions prepared from **2** and **5**. Although DLS results showed small variations in the average size of the aggregates (Figure S3 in the ESM), these compounds were able to form stable aggregates for at least three months at f_w of 80 and 90%, respectively.

3.2 Preparation and characterization of micro- and nanocrystals

Taking advantage of the AIEE behavior and the high stability that the aggregates of **2** and **5** showed in THF/water mixtures, both Pt(II) compounds were selected to fabricate micro- and nanocrystals using the oil-in-water (O/W) droplets as a template [34]. As described above, the addition of small amounts of water over a THF solution of the Pt(II) compound generates water-in-oil (W/O) droplets, which can be inverted to an O/W system by further increasing the water content of the solvent mixtures (Figure 3(a,b)). As a result, the Pt(II) compound is self-assembled into micelle-like aggregates around the water-oil interface in order to avoid precipitation (Figure 3(c)). Keep in mind that these compounds are not soluble in water due to the functionalization of the benzene moiety with terminal alkyl chains. Nonetheless, the formed aggregates show a high stability and are able to maintain its spherical structure even after the THF is removed by slow evaporation, giving rise to the micro- and nanocrystals as confirmed by TEM (Figure 3(d)).

When preparing these materials, it is essential to consider that the droplet size will directly affect to the final diameter of the crystals because droplets will act as a template [35]. Thus, several methods and conditions were previously tested for studying the effect of several parameters in the droplet size, such as the temperature, the stirring speed, the reaction vessel, and the synthetic procedure.

Figure 4(a) displays the emission spectra of **2** in the O/W droplets formed by manual shaking from mixtures with f_w = 80%, and stabilized at selected temperatures. The ^{3}MMLCT emission band appears centered at 624 nm in all cases, in agreement with the formation of Pt···Pt aggregates. Additionally, a weak band is also recorded at *ca*. 500 nm when the droplets are stabilized at 4ºC, which evidences the presence of Pt(II) species in their monomer form. Most likely, the low temperature causes a destabilization of the self-assembled structures, and some of them are broken, releasing the molecules to the solution. The size of the corresponding aggregates was analyzed by DLS, as demonstrated in Figure 4(b). Results do not show significant changes in the size distributions, the Z-Average and PDI values being at around 234 nm and 0.17 for the three solutions.

Another key factor that can have a great influence on the droplet size is the stirring speed during the addition of water over the THF solution. To analyze the self-assembly behavior of **2** and the diameter of the corresponding aggregates, the O/W droplets were formed by manual shaking, by stirring at 300, 600 and 1300 rpm, and under sonication. As shown in Figure 4(c) and S4(a), stable aggregates can be obtained in the two first cases, whereas sonication leads to a considerable damage and all the aggregates are destroyed. In the particular case of magnetic stirring, speeds relatively low or moderate of 300 and 600 rpm are the most suitable to achieve dispersions with high emission intensity. By contrast, the assembly of the Pt(II) compounds seems not to be as effective at higher speeds of 1300 rpm. DLS measurements support these features and suggest that the O/W droplets can be split in other smaller by increasing the energy of the mechanical stirring. Thus, for example, magnetic stirring at 300 rpm allows obtaining smaller and well-dispersed aggregates (Z-Average: 234 nm; PDI: 0.071) than

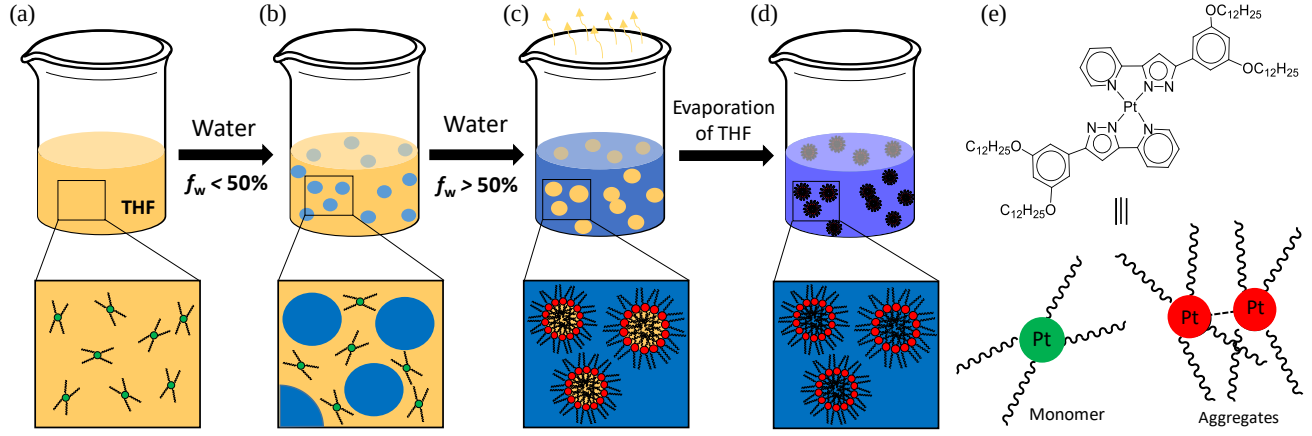

Figure 3 Schematic representation of the droplet method used for obtaining micro- and nanocrystals. (a) THF solution of the hydrophobic Pt(II) compound (10^{-3} M). (b) Formation of W/O droplets. (c) Inversion of a W/O to an O/W system, and formation of micellar-like Pt(II) aggregates. (d) Removal of the oil phase to obtain the micro- and nanocrystals. (e) Molecular structure of **2**, and schematic drawings of its assemblies in the monomer or aggregated forms. Pyrazolate ligands have been not schematically drawn for the sake of clarity.

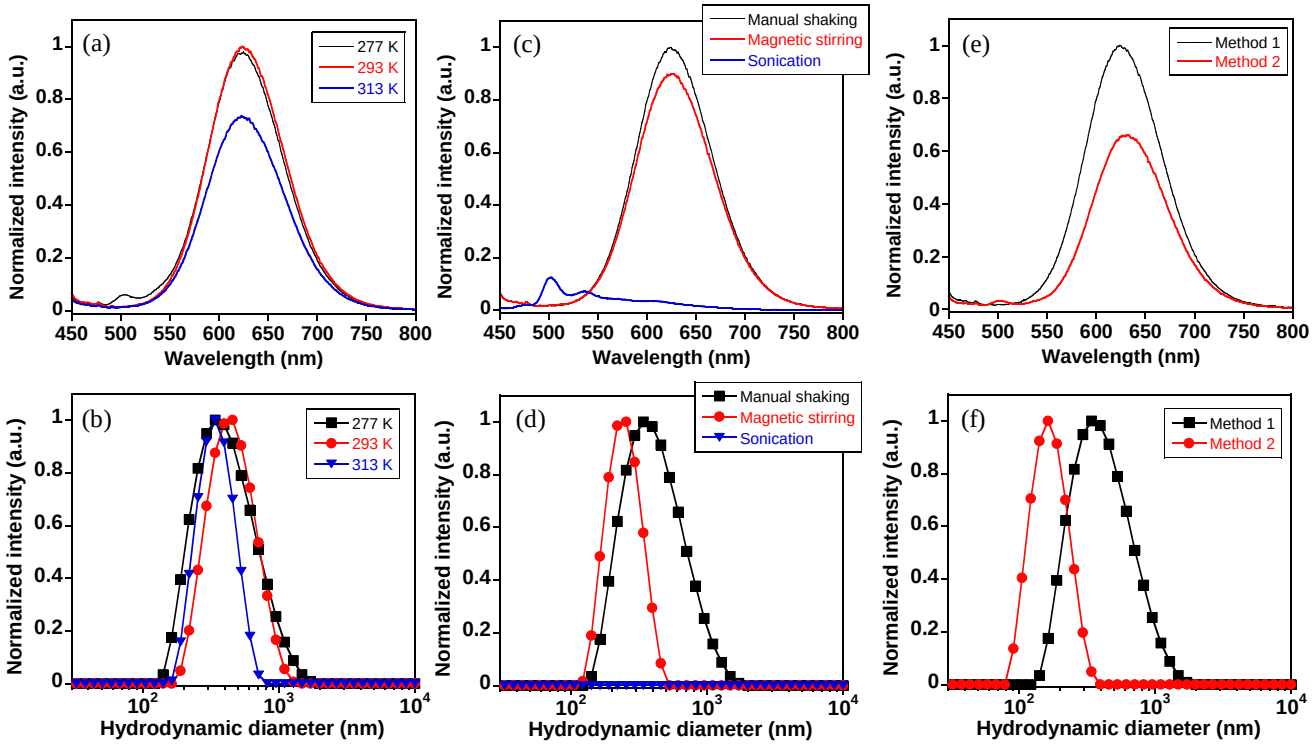

Figure 4 Emission spectra and DLS analysis for the O/W droplets containing the Pt(II) compound **2** obtained under different (a,b) stabilization temperatures, (c,d) stirring speeds, and (e,f) preparation methods. All droplets were prepared from THF/water mixtures with f_w = 80 %.

those formed by manual shaking (Z-Average: 290.7 nm; PDI: 0.2) (Figure 4(d)). These results also demonstrate that the speed of the magnetic stirrer has not a remarkable effect in the average droplet size, obtaining values of 233 nm (PDI: 0.04) and 207 nm (PDI: 0.06) when speed reaches 600 and 1300 rpm,

respectively (Figure S4(b) in the ESM).

We were also interested in exploring how the reaction vessel affects to the droplet size because hitherto, only typical vials with a section of 22 mm have been used to form the O/W droplets. In Figure S5, it is plotted the DLS analysis and the emission spectrum for the dispersion of droplets of **2** prepared at room temperature after the addition of water over THF at 300 rpm, but using a round-bottom flask of 25 mL. As observed, both the droplet size and the PDI notably increase, reaching average values of 715 nm and 0.15, respectively. Regarding the luminescence properties, the emission band centered at 630 nm evidences the formation of aggregates, but its intensity is rather low, which could be an indication of a weakening of the intermolecular Pt(d_{z^2})···Pt(d_{z^2}) interactions due to the increase in droplet size.

At this point of the work, note that we have always used the same method to create the O/W droplets, which is based in the addition of water over the THF solution containing the prototype Pt(II) compound (Method 1). Thus, the O/W droplets are formed by an inversion process that occurs when f_w reaches values above 50-60% (see Figure 3). However, it is easy to obtain the O/W droplets by slow addition of the THF solution over water (Method 2) [36]. This direct method, in combination with magnetic stirring, offers to the possibility for obtaining luminescent aggregates even smaller with an average size of 160 nm and a PDI of 0.085 (Figure 4(e,f)).

On the basis of the above-discussed studies, several micro- and nanocrystals were prepared from THF/water mixtures of **2** (f_w = 80 %) upon the next conditions: (a) Method 1 (magnetic stirring; T = 20 ºC); (b) Method 2 (magnetic stirring; T = 20 ºC); (c) Method 1 (magnetic stirring; T = 4 ºC) (see Experimental section for more details). In all cases, evaporation of THF gave stable colloidal dispersions that exhibit a bright orange emission (Figure S6 in the ESM). The DLS measurements show similar results to those found in the initial O/W droplets used as template, which suggests that the structure of the Pt(II) aggregates is maintained after THF evaporation. Methods 1 and 2 with a droplet stabilization at room temperature allow obtaining microcrystals with a Z-Average of 246.0 nm and 205.8 nm, respectively (Figure 5(a,b)). Although these values seem to be similar, note that method 2 gives highly monodisperse particles with a PDI value of 0.04. Otherwise, when the droplets formed by method 1 are stabilized at 4ºC, a bimodal size distribution is clearly observed with mean values of 95.4 nm and *ca.* 500 nm (Figure 5(c)). This fact is rather surprisingly because the smaller distribution was not observed in the DLS experiments of the initial O/W droplets (see Figure 4(b)). The results seem to indicate that the nanocrystals with a hydrodynamic diameter of around 95 nm are majority and have good monodispersity. This effect by temperature was also observed in the O/W droplets prepared via method 2.

To analyze the morphology of the micro- and nanocrystals, low-resolution TEM studies were also carried out. As shown in Figure 5(d-f), microphotographs display well-defined spherical particles with a core-shell type structure, which undoubtedly confirms the formation of the Pt···Pt aggregates. It is interesting to note that during the self-assembly process in the O/W droplets, the terminal alkyl chains of the coordinated pyrazolate ligands fall in opposite directions, i.e. some of them point outwards, and other ones are located within the core, in contact with THF [37]. In the TEM images, the organic ligands including the terminal alkyl chains pointing out are clearly observed in the form of a low-contrast shell with a non-regular contour. Regarding to the particle size, TEM analysis are in agreement with the results found by DLS. For the microcrystals obtained from methods 1 and 2 with a droplet stabilization at room temperature, the average diameter of the core (D_c) is measured to be 206.1 ± 74.3 nm and 196.2 ± 37.2 nm, respectively, which fits well with the corresponding hydrodynamic diameters (Figure 5(g,h)). By contrast, stabilization at 4 ºC reduces the mobility of the droplets and hinders the coalescence processes, obtaining small nanocrystals with an average diameter of 58.3 ± 12.2 nm (Figure 5(f)). In agreement with the bimodal size distribution recorded by DLS, it is also observed the existence of some bigger aggregates with a diameter of *ca.* 500 nm (Figure S7 in the ESM). These particles are probably originated as a result of the self-assembly of the Pt(II) compounds into coalesced O/W droplets and represent less than 2%. The preparation of the O/W droplets by immersion in an ice-water bath notably reduces the number of these aggregates. On the other

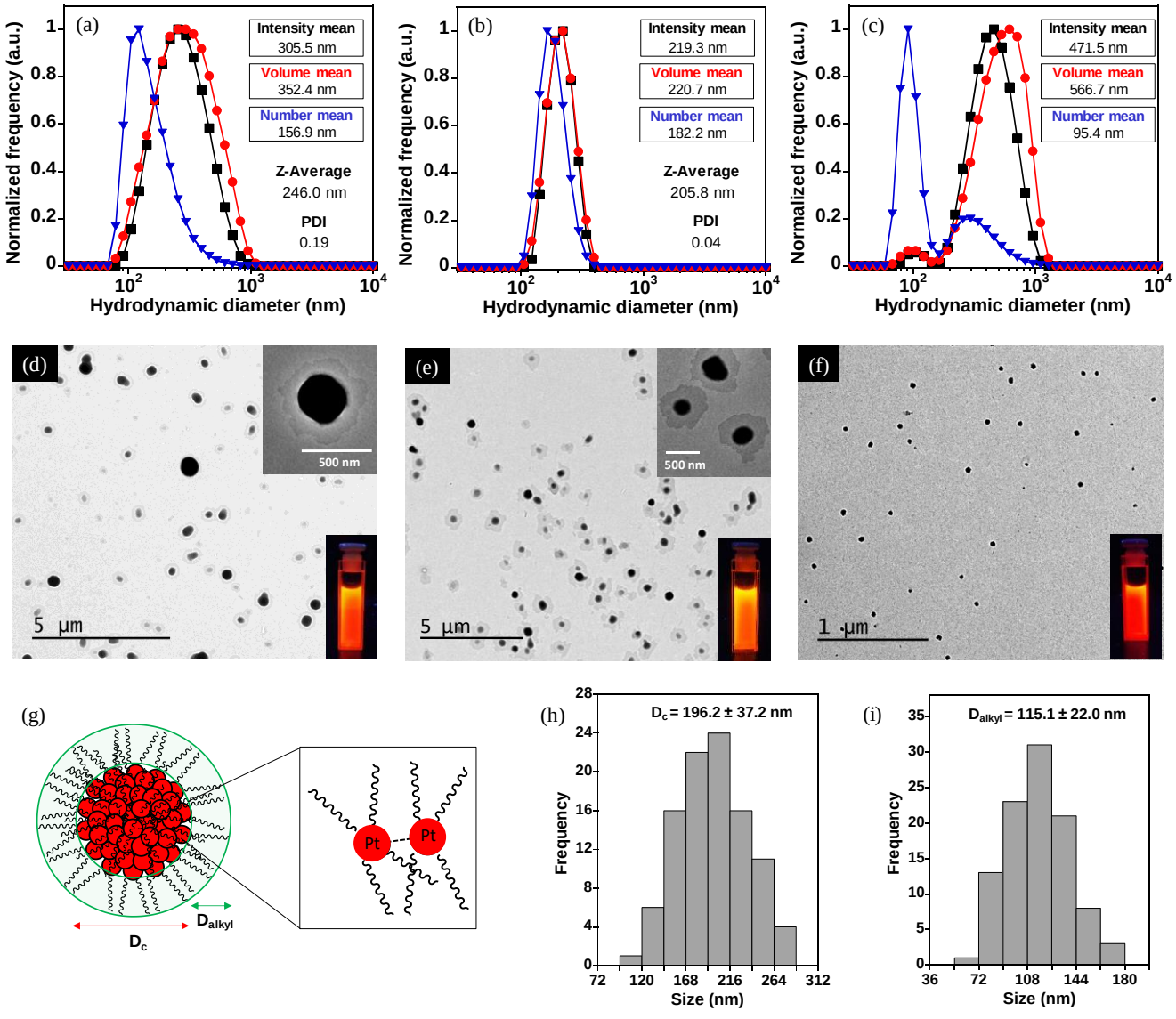

Figure 5 DLS analysis for the micro- and nanocrystals of **2** synthesized via (a) method 1 with droplet stabilization at 20ºC, (b) method 2 with droplet stabilization at 20 ºC, and (c) method 1 with droplet stabilization at 4 ºC. (d,e,f) The corresponding TEM images of the synthesized micro- and nanocrystals of **2**. The insets display a detail of the particle morphology and the orange emission observed under UV light ($\lambda_{exc.}$ = 365 nm). (g) Schematic drawing showing the self-assembly of the Pt(II) compounds in the synthesized crystals. (h,i) Core and shell size distribution histograms for the microcrystals obtained *via* method 2.

hand, the size of the shell containing the alkyl chains (D_{alkyl}) was also analyzed, showing in all cases similar values ranging between 95 and 115 nm (Figure 5(i)).

Microcrystals of **2** prepared by method 1 at 25 ºC were selected as a prototype for powder X-ray diffraction studies. As shown in Figure S8, the diffractogram displays a series of four well-defined peaks in the small-angle region with a reciprocal *d*-spacing ratio of 1 : 1/2 : 1/3 : 1/4, which is consistent with a lamellar distribution of the Pt(II) compounds in the micellar-like assemblies. In addition, another broad peak with a *d*-spacing of 3.2 Å is recorded at around 28º; this reflection is attributed to the inter-aggregate distance and supports the establishment of intermolecular Pt···Pt interactions.

The self-assembly behavior of compound **5** in the O/W droplets was also investigated. Taking into account the experiments previously performed with

2 regarding to the droplet size, the new particles were prepared *via* method 1 under magnetic stirring both at 20 and 4 ºC. The droplets again showed an excellent ability to act as templates because only small variations in the size and in the emission band were observed between the final crystals and the initial O/W droplets. As observed in Figure S9(a), method 1 at 20 ºC gives monodisperse microcrystals with a hydrodynamic diameter of 133.8 nm and a PDI value of 0.09, which is confirmed by TEM (Figure 6(a,b)). Interestingly, since compound **5** has short terminal alkyl chains of four carbon atoms, it allows obtaining smaller particles than those prepared from **2** upon the same conditions. Also, note that the shell attributed to the alkyl chains is not observed by TEM due to its small size.

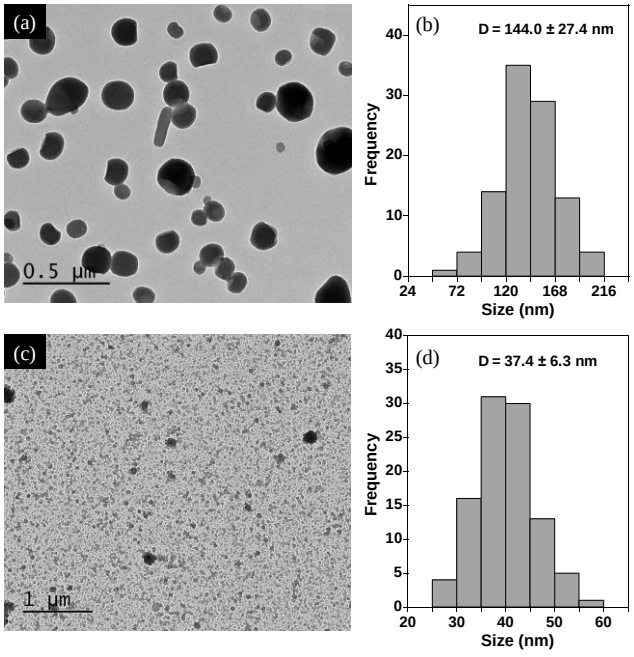

Figure 6 (a,b) TEM microphotograph showing the microcrystals of 5 obtained by stabilization of the O/W droplets at 20 ºC, and particle size distribution histogram. (c,d) TEM microphotograph showing the nanocrystals of 5 obtained by stabilization of the O/W droplets at 4 ºC, and particle size distribution histogram.

Otherwise, the stabilization of droplets at 4 ºC causes a dramatic decrease of the final particle size, as expected, obtaining nanocrystals with an average size of 37.4 ± 6.3 nm (Figure 6(c,d)). Although the particles are highly monodisperse, some higher aggregates of *ca*. 340 nm are also observed by TEM. This fact can be explained by considering the high ease of aggregation of these nanoparticles since the steric repulsions among the alkyl chains decrease as a consequence of their small length. The DLS measurements also confirm the presence of these aggregates in solution (Figure S9(b)).

3.3 Colloidal and thermal stability

The colloidal stability of the aqueous dispersions containing the micro- and nanocrystals of **2** and **5** was evaluated for three months. On the one hand, DLS measurements were performed to detect potential changes in the size of crystals that could be originated by aggregation processes or as a result of the precipitation of the Pt(II) compounds. On the other hand, emission spectra were also recorded in order to visualize the changes that the loss of the assembly can originate in the emission intensity. In general terms, it should be noted that most of the colloidal dispersions are stables for at least three months, the particle-size distributions showing no remarkable changes (Figure 7(a)). Regarding to the luminescence properties, it is observed that the emission intensity progressively decreases over time because of the quenching effect of oxygen, but crystals continue to emit a bright orange light with the emission maximum at around 600 – 630 nm, which indicates that molecules remain assembled in the aggregated form (Figure 7(b)). However, in the particular case of the crystals of **2** obtained from the droplets stabilized by method 1 at 20 ºC, DLS and photophysical results indicate that the self-assembly of the Pt(II) compounds is unstable, and total precipitation occurs in less than a week (Figure S10). The thermal stability of the colloidal dispersions was also evaluated in the temperature range of 20 – 80 ºC. As shown in Figure 7(d) for two selected dispersions of microcrystals, the hydrodynamic diameter remains constant during the overall thermal process. This result is an indication that the crystals are highly stable in a wide temperature range. As expected, the emission intensity decreases with the increase of temperature in agreement with the existence of thermally-activated non-radiative processes [38], but the emission band is maintained at around 600 – 630 nm, confirming the results from DLS (Figure 7(e)). The initial emission intensity is practically recovered when the colloidal dispersion back to room

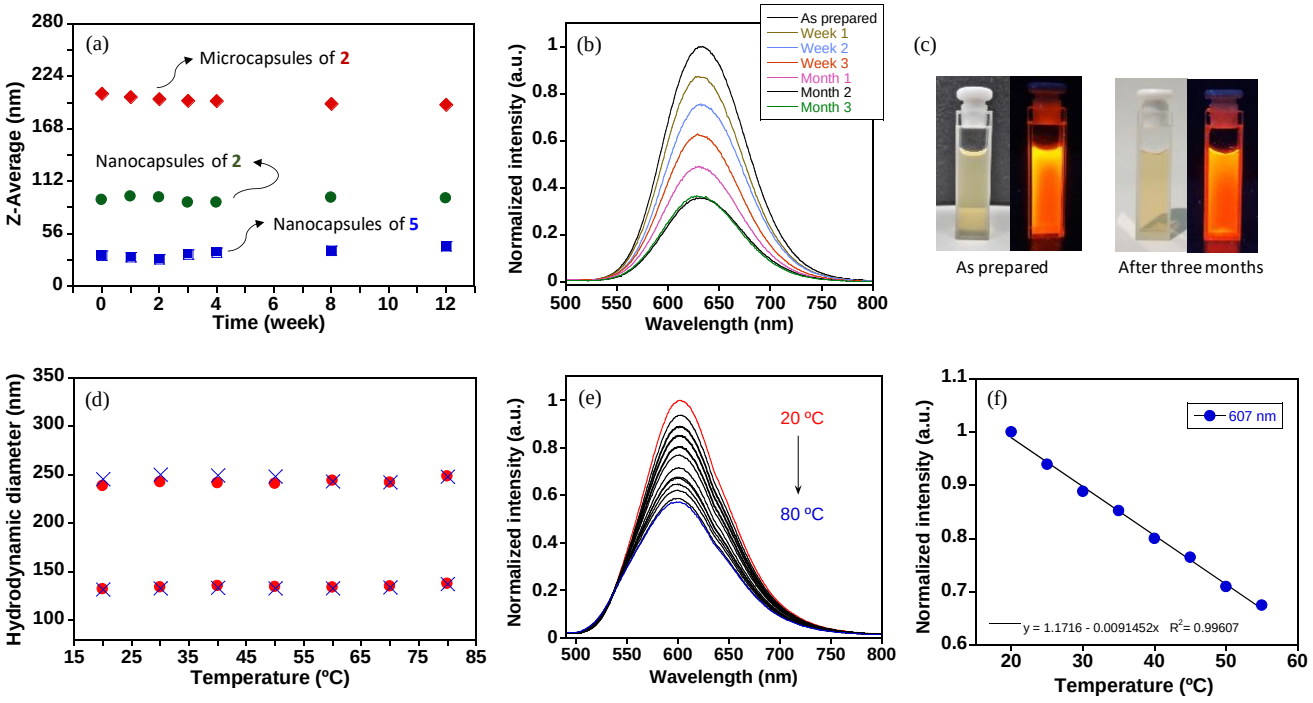

Figure 7. Colloidal stability of the micro- and nanocrystals: (a) Changes in the particle size measured by DLS over time for the microcrystals of **2** (method 2, droplet stabilization at 20 ºC), nanocrystals of **2** (method 1, droplet stabilization at 4 ºC), and nanocrystals of **5** (method 1, droplet stabilization at 4 ºC). The Z-average was obtained from the hydrodynamic diameter for the microcrystals, and from the number mean in the case of the nanocrystals; (b) Fluorescence stability of the microcrystals obtained from **2**; (c) Images showing the orange emission of the colloidal dispersions of microcrystals of **2** as prepared and after three months, taken with the naked eye (left) and under UV light (right). Thermal stability of the microcrystals obtained *via* method 1: (d) Changes in the hydrodynamic diameter of microcrystals prepared from **2** and **5** measured by DLS as a function of temperature; (e) Temperature-dependent emission spectra of microcrystals of **5** upon heating; (f) Emission intensity of microcrystals of **5** as a function of temperature recorded upon heating. The linear regression and its corresponding equation are also shown.

temperature. Also note that the luminescence response of the crystals shows a clear linear tendency with temperature, so that it could be possible to measure the temperature of the environment close to the particles by the linear regression method (Figure 7(f)). This could be of great interest in the field of biomedicine as a cellular temperature monitoring system.

3.4 Encapsulation efficiency

The ability of the hollow micro and nanocrystals for the entrapment of highly hydrophobic drugs was assessed by using coumarin 6 (C6) as a model. C6 is a fluorescent dye that emits an intense green light in THF solution, as demonstrated in Figure S11. Its solubility in water, however, is almost negligible and consequently C6 forms non-emissive microcrystals in aqueous solutions (Figure S11) [39]. This coumarin is frequently used as a model for hydrophobic drug encapsulation because it is possible detect quickly if C6 has been trapped in a lipid-like environment, simply by analyzing the luminescence properties of the aqueous dispersions [40-42].

C6-loaded microcapsules were prepared from a THF solution of **2** and C6 *via* method 2, i.e. by adding the oil phase over water to form O/W droplets (Figure 8(a)). In the first stage, the molecules of **2** are self-assembled around the droplets through intermolecular Pt···Pt interactions and C6 is trapped inside. This fact is supported by the presence of two bands in the emission spectrum of the aqueous solution containing the O/W droplets (Figure 8(b)). The band centered at 512 nm is associated with the presence of C6 solved in THF, which demonstrates that the hydrophobic drug is located inside the droplets. Otherwise, it can be also observed at around 624 nm the typical broad band of **2** in its

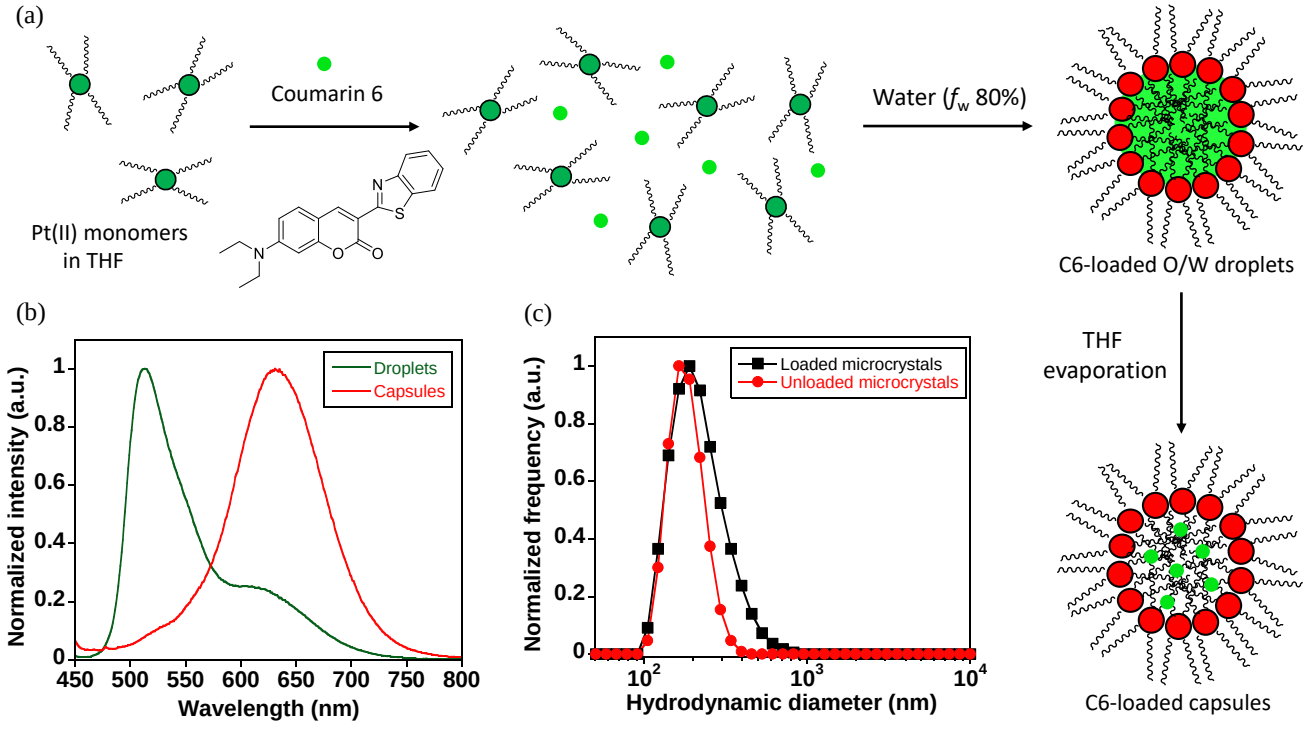

Figure 8. (a) Schematic drawing showing the strategic route for C6 entrapment inside the Pt(II)-based capsules. (b) Normalized emission spectra of the aqueous dispersions containing the C6-loaded O/W droplets and capsules prepared from **2** (method 2 with droplet stabilization at 20 ºC). (c) DLS number size distribution for the C6-loaded microcapsules of **2**. Unloaded microcrystals are also plotted for comparison.

self-assembled form. In the second stage, evaporation of THF causes the crystallization of C6 inside the Pt(II)-based microcapsules, which originates the quenching of its natural greenish emission (Figure 8(b)). Encapsulation efficiency and drug loading were calculated by UV-Vis spectrophotometry, obtaining values of 79 % and 16 %, respectively (Table S2 in the ESM). DLS measurements were also carried out to analyze the size and ζ-potential of the C6-loaded capsules. As shown in Figure 8(c), entrapment of C6 produces an increase of the average size from 205.8 to 311.6 nm, as well as an increase in the polydispersity index, which now achieves values of *ca*. 0.2 (the PDI value of the unloaded microcapsules is 0.04). By contrast, no remarkable variations were found in the ζ-potential, whose value was found to be -34.9 mV.

Similar experiments were performed to prepare C6-loaded microcrystals *via* method 1, but the addition of water over the THF solution of **2** and C6 causes the precipitation of both compounds and prevents the stabilization of **2** in its self-assembled form.

Entrapment studies were also carried out using the Pt(II) compound **5** decorated with short alkyl chains to obtain C6-loaded microcrystals *via* method 2, but encapsulation was only achieved with less than 5% of efficiency (Table S2 in the ESM). Most likely, the alkyl chain length is not enough long to achieve the retention of C6 inside the capsules.

The effect of the size particle was also analyzed by preparing C6-loaded nanocapsules from compound **2** via method 2 at 4 ºC. The encapsulation efficiency was estimated to be 26%, and nanocapsules showed a drug-loading capacity of *ca.* 5% (Table S2 in the ESM). As expected, the ability of the nanocrystals of **2** to encapsulate C6 is lower than that found in the analogous microcrystals of **2** (79%), which can be attributed to the decrease of the available space in the internal cavity of these nanocrystals.

In summary, there are two key factors that have a great influence on the retention of C6 inside the

capsules: the alkyl chain length and the particle size. On the basis of the above results, we can establish that the best capsules for entrapment of C6 are those synthesized from compound **2** decorated with long alkyl chains via method 2 at room temperature.

4 Conclusions

We have demonstrated that discotic Pt(II) metallomesogens can be well-dispersed in water despite their great hydrophobic nature. THF/water mixtures form oil-in-water droplets with average sizes ranging between 40 and 250 nm, in which the Pt(II) compounds are confined and driven to be self-assembled *via* intermolecular Pt···Pt interactions to avoid precipitation. This interaction concomitantly causes an aggregation-induced emission enhancement as a consequence of the formation of ^{3}MMLCT excited states. Taking advantage of the droplets as a template, luminescent aqueous dispersions of hollow micro- or nanocrystals have been successfully obtained by slow THF evaporation. The Pt(II) compounds maintain their self-assembled form and their bright orange emission, exhibiting a high thermal and colloidal stability for at least 80 ºC and three months, respectively. Moreover, since the core of these particles is hollow, they can act as nanocapsules for entrapment of hydrophobic drugs, which has been successfully proved by using coumarin-6 as a model. The Pt(II) microcrystals show the highest values of encapsulation efficiency at around 80 %, with a drug loading capacity of 16 %. These results open a new way to achieve the dispersion of hydrophobic Pt(II) metallomesogens in water, which could be of great interest for biomedical applications.

Acknowledgements

This work was supported by the Associate Laboratory for Green Chemistry – LAQV, which is financed by national funds from FCT/MCTES (UIDB/50006/2020), and the PROTEOMASS Scientific Society (general funds). C. Cuerva acknowledges the Spanish Foundation Alfonso Martín Escudero for his postdoctoral fellowship. JF-L thanks FCT/MEC (Portugal) the junior researcher contract under DL/57 programme.

Electronic Supplementary Material: Supplementary material (luminescence properties and DLS analysis of the O/W droplets, photophysical characterization of micro and nanocrystals of **2** and **5**, TEM analysis of nanocrystals of **2**, XRD studies for microcrystals of **2**, DLS analysis of micro- and nanocrystals of **5**, time-dependent emission spectra of microcrystals of **2**, emission spectra of coumarin 6, encapsulation efficiency and drug-loading capacity data) is available in the online version of this article at http://dx.doi.org/10.1007/s12274-***-****-* (automatically inserted by the publisher).

References

[1] Jenekhe, S. A.; Osaheni, J. A. Excimers and exciplexes of conjugated polymers. *Science* **1994**, 265, 765–768.

[2] Zhao, N.; Lam, J. W. Y.; Sung, H. H. Y.; Min Su, H.; Williams, I. D.; Wong, K. S.; Tang, B. Z. Effect of the counterion on light emission: a displacement strategy to change the emission behaviour from aggregation - caused quenching to aggregation - induced emission and to construct sensitive fluorescent sensors for Hg^{2+} detection. *Chem. Eur. J.*, **2014**, 20, 133-138.

[3] Qi, J.; Hu, X.; Dong, X.; Lu, Y.; Lu, H.; Zhao, W.; Wu, W. Towards more accurate bioimaging of drug nanocarriers: turning aggregation-caused quenching into a useful tool. *Adv. Drug Deliv. Rev.*, **2019**, 143, 206-225.

[4] Wu, H.; Zhang, L.; Yang, J.; Bo, R.; Du, H.; Lin, K.; Zhang, D.; Ramachandran, M.; Shen, Y.; Xu, Y.; Xue, X.; Ma, Z.; Lindstrom, A. R.; Carney, R.; Lin, T.-Y.; Li, Y. Rotatable aggregation - induced - emission/aggregation - caused - quenching ratio strategy for real - time tracking nanoparticle dynamics. *Adv. Funct. Mater.*, **2020**, https://doi.org/10.1002/adfm.201910348

[5] Wang, H.; Zhao, E.; Lam, J. W. Y.; Tang, B. Z. AIE luminogens: emission brightened by aggregation. *Mater. Today*, **2015**, 18, 365-377

[6] Tian, W.; Zhang, J.; Yu, J.; Wu, J.; Nawaz, H.; Zhang, J.; He, J.; Wang, F. Cellulose - based solid fluorescent materials. *Adv. Opt. Mater.*, **2016**, 4, 2044-2050

[7] Hu, R.; Leung, N. L. C.; Tang, B. Z. AIE macromolecules: syntheses, structures and functionalities. *Chem. Soc. Rev.*, **2014**, 43, 4494-4562.

[8] Hong, Y.; Lama, J. W. Y.; Tang, B. Z. Aggregation-induced emission: phenomenon, mechanism and applications. *Chem. Commun.*, **2009**, 4332-4353.

[9] Luo, J.; Xie, Z.; Lam, J. W. Y.; Cheng, L.; Chen, H.; Qiu, C.; Kwok, H. S.; Zhan, X.; Liu, Y.; Zhu, D.; Tang, B. Z. Aggregation-induced emission of 1-methyl-1,2,3,4,5-pentaphenylsilole. *Chem. Commun.*, **2001**, 1740.

[10] Tang, B. Z.; Zhan, X.; Yu, G.; Lee, P. P. S.; Liu, Y.; Zhu, D. Efficient blue emission from siloles. *J. Mater. Chem.*, **2001**, 11, 2974.

[11] Guo, Z.; Yan, C.; Zhu, W.-H. High - performance quinoline - malononitrile core as a building block for the diversity - oriented synthesis of AIEgens. *Angew. Chem. Int. Ed.*, **2020**, doi:10.1002/anie.201913249.

[12] Chen, Z.; Zhang, J.; Song, M.; Yin, J.; Yu, G.-A.; Liu, S. H. A novel fluorene-based aggregation-induced emission (AIE)-active gold(i) complex with crystallization-induced emission enhancement (CIEE) and reversible mechanochromism characteristics**.** *Chem. Commun.*, **2015**, 51, 326-329.

[13] Zhao, F.; Chen, Z.; Fan, C.; Liu, G.; Pu, S. Aggregation-induced emission (AIE)-active highly emissive novel carbazole-based dyes with various solid-state fluorescence and reversible mechanofluorochromism characteristics. *DyesPigments*, **2019**, 164, 390-397.

[14] Hou, X.-G.; Wu, Y.; Cao, H.-T.; Sun, H.-Z.; Li, H.-B.; Shan, G.-G.; Su, Z.-M. A cationic iridium(III) complex with aggregation-induced emission (AIE) properties for highly selective detection of explosives. *Chem. Commun.*, **2014**, 50, 6031-6034.

[15] Gao, H.; Xu, D.; Wang, Y.; Wang, Y.; Liu, X.; Han, A.; Zhang, C. Effects of alkyl chain length on aggregation-induced emission, self-assembly and mechanofluorochromism of tetraphenylethene modified multifunctional β-diketonate boron complexes. *DyesPigments*, **2018**, 150, 59-66.

[16] Chowdhury, A.; Howlader, P.; Mukherjee, P. S. Aggregation - induced emission of platinum(II) metallacycles and their ability to detect nitroaromatics. *Chem. Eur. J.*, **2016**, 22, 7468-7478.

[17] Li, P.; Zeng, Q.-Y.; Sun, H.-Z.; Akhtar, M.; Shan, G.-G.; Hou, X.-G.; Li, F.-S.; Su, Z.-M. Aggregation-induced emission (AIE) active iridium complexes toward highly efficient single-layer non-doped electroluminescent devices. *J. Mater. Chem. C*, **2016**, 4, 10464-10470.

[18] Proetto, M. T.; Sanning, J.; Peterlechner, M.; Thunemann, M.; Stegemann, L.; Sadegh, S.; Devor, A.; Gianneschi, N. C.; Strassert, C. A. Phosphorescent Pt(II) complexes spatially arrayed in micellar polymeric nanoparticles providing dual readout for multimodal imaging. *Chem. Commun.*, **2019**,55, 501-504.

[19] Wu, Y.; Tan, X.; Lv, A.; Yu, F.; Ma**,** H.; Shen, K.; Sun, Z.; Chen, F.; Chen, Z.-K.; Hang, X.-C. Triplet excited-state engineering of phosphorescent Pt(II) complexes. *J. Phys. Chem. Lett.* **2019**, 10, 5105-5110

[20] Li, K.; Tong, G. S. M.; Wan, Q.; Cheng, G.; Tong, W.-Y.; Ang, W.-H.; Kwong, W.-L.; Che, C.-M. Highly phosphorescent platinum(II) emitters: photophysics, materials and biological applications. *Chem. Sci.*, **2016**, 7, 1653-1673

[21] Liu, L.; Wang, X.; Wang, N.; Peng, T.; Wang, S. Bright, Multi-responsive, Sky-Blue Platinum(II) Phosphors Based on a Tetradentate Chelating Framework. *Angew. Chem. Int. Ed.*, **2017**, 24, 9160-9164.

[22] Ganesan, P.; Hung, W.-Y.; Tso, J.-Y.; Ko, C. - L.; Wang, T.-H.; Chen, P. - T.; Hsu, H. - F.; Liu, S. - H.; Lee, G. - H.; Chou, P. - T.; Jen, A. K. - Y.; Chi, Y. Functional pyrimidinyl pyrazolate Pt(II) complexes: role of nitrogen atom in tuning the solid - state stacking and photophysics. *Adv. Funct. Mater.*, **2019**, 29, 1900923

[23] Fu, T.-F.; Ao, L.; Gao, Z.-C.; Zhang, X.-L.; Wang, F. Advances on supramolecular assembly of cyclometalated platinum(II) complexes. *Chin. Chem. Lett.*, **2016**, 27, 1147-1154.

[24] Wu, J.; Li, Y.; Tan, C.; Wang, X.; Zhang, Y.; Song, J.; Qu, J.; Wong, W.-Y. Aggregation-induced near-infrared emitting platinum(II) terpyridyl complex: cellular characterisation and lysosome-specific localisation. *Chem. Commun.*, **2018**, 54, 11144-11147.

[25] Gao, L.; Ni, J.; Su, M.; Kang, J.; Zhang, J. Luminescence switching property of cycloplatinated(II) complexes bearing 2-phenylpyridine derivatives and the application for data security storage. *DyesPigments*, **2019**, 165, 231-238.

[26] Chan, K. T.; Tong, G. S. M.; To, W.-P.; Yang, C.; Du, L.; Phillips, D. L.; Che, C.-M. Highly phosphorescent platinum(II) emitters: photophysics, materials and biological applications. *Chem. Sci.*, **2016**, **7**, 1653-1673.

[27] Cuerva, C.; Campo, J. A.; Ovejero, P.; Torres, M. R.; Oliveira, E.; Santos, S. M.; Lodeiro, C.; Cano, M. Columnar discotic Pt(II) metallomesogens as luminescence multifunctional materials with chemo and thermosensor abilities**.** *J. Mater. Chem. C*, **2014**, 2, 9167-9181.

[28] Cuerva, C.; Campo, J. A.; Cano, M.; Lodeiro, C. Platinum(II) metallomesogens: new external - stimuli - responsive photoluminescence materials. *Chem. Eur. J.*, **2016**, 22, 10168-10178.

[29] Cuerva, C.; Campo, J. A.; Cano, M.; Lodeiro, C. Multi - stimuli - responsive properties of aggregation - enhanced emission - active unsymmetrical Pt^{II} metallomesogens through self - assembly. *Chem. Eur. J.*, **2019**, 25, 12046-12051.

[30] Cuerva, C.; Campo, J. A.; Cano, M.; Caño-García, M.; Otón, J. M.; Lodeiro, C. Aggregation-induced emission enhancement (AIEE)-active Pt(II) metallomesogens as dyes sensitive to Hg^{2+} and dopant agents to develop stimuli-responsive luminescent polymer materials. *DyesPigments*, **2020**, 175, 108098.

[31] Giménez, N.; Lalinde, E.; Lara, R.; Moreno, M. T. Design of luminescent, heteroleptic, cyclometalated Pt^{II} and Pt^{IV} complexes: photophysics and effects of the cyclometalated ligands. *Chem. Eur. J.*, **2019**, 25, 5514-5526.

[32] Chang, S.-Y.; Kavitha, J.; Hung, J.-Y.; Chi, Y. Luminescent platinum(II) complexes containing isoquinolinyl indazolate ligands: synthetic reaction pathway and photophysical properties. *Inorg. Chem.* **2007**, 46, 7064-7074.

[33] Ku, H.-Y.; Tong, B.; Chi, Y.; Kao, H.-C.; Yeh, C.-C.; Chang, C.-H.; Lee, G.-H. Luminescent Pt(II) complexes bearing dual isoquinolinyl pyrazolates: fundamentals and applications. *Dalton Trans.*, **2015**, 44, 8552-8563.

[34] Ogasawara, M.; Lin, X.; Kurata, H.; Ouchi, H.; Yamauchi, M.; Ohba, T.; Kajitani, T.; Fukushima, T. Numata, M.; Nogami, R.; Adhikaria, B.; Yagai, S. Water-induced self-assembly of an amphiphilic perylene bisimide dyad into vesicles, fibers, coils, and rings. *Mater. Chem. Front.*, **2018**, 2, 171.

[35] Sun, Y.; Mei, L.; Han, N.; Ding, X.; Yu, C.; Yang, W.; Ruan, G. Examining the roles of emulsion droplet size and surfactant in the interfacial instability-based fabrication process of micellar nanocrystals. *Nanoscale Res. Lett*., **2017**, 12, 434.

[36] Piorkowski, D. T.; McClements, D. J. Beverage emulsions: Recent developments in formulation, production, and applications. *Food Hydrocoll.*, **2014**, 42, 5-41.

[37] Aliprandi, A.; Mauro, M.; De Cola, L. Controlling and imaging biomimetic self-assembly. *Nat. Chem.*, **2016**, 8, 10-15.

[38] Liao, C. T.; Chen, H. H.; Hsu, H. F.; Poloek, A.; Yeh, H. H.; Chi, Y.; Wang, K. W.; Lai, C. H.; Lee, G. H.; Shih, C. W.; Chou, P. T. Mesomorphism and luminescence properties of platinum(II) complexes with tris(alkoxy)phenyl - functionalized pyridyl pyrazolate chelates. *Chem. Eur. J.*, **2011**, 17, 546-556.

[39] Banerjee, R.; Purkayastha, P. Revival of the nearly extinct fluorescence of coumarin 6 in water and complete transfer of energy to rhodamine 123**.** Soft Matter, **2017**, 13, 5506-5508.

[40] Banerjee, R.; Mondal, S.; Purkayastha, P. Revival, enhancement and tuning of fluorescence from Coumarin 6: combination of host–guest chemistry, viscosity and collisional quenching. *RSC Adv.*, **2016**, 6, 105347-105349.

[41] Banerjee, R.; Sinha, R.; Purkayast, P. β-Cyclodextrin encapsulated coumarin 6 on graphene oxide nanosheets: impact on ground-state electron transfer and excited-state energy transfer**.** *ACS Omega*, **2019**, 4, 16153-16158

[42] Ma, W.; Chen, M.; Kaushal, S.; McElroy, M.; Zhang, Y.; Ozkan, C.; Bouvet, M.; Kruse, C.; Grotjahn, D.; Ichim, T.; Minev, B. PLGA nanoparticle-mediated delivery of tumor antigenic peptides elicits effective immune responses. *Int. J. Nanomedicine*, **2012**, 7, 1475–1487.

Electronic Supplementary Material

Water-soluble hollow nanocrystals from self-assembly of AIEE-active Pt(II) metallomesogens

Cristián Cuerva[1] (✉), Javier Fernández-Lodeiro[1,2], Mercedes Cano[3], José Luis Capelo-Martínez[1,2] Carlos Lodeiro[1,2] (✉)

[1] *BIOSCOPE Research Group, LAQV@REQUIMTE Chemistry Department, NOVA School of Science and Technology, NOVA University Lisbon, 2829-516 Caparica (Portugal). E-mail: c.alaiz@fct.unl.pt; cle@fct.unl.pt*
[2] *PROTEOMASS Scientific Society, Rua dos Inventores, Madam Parque, Caparica Campus, 2829-516 Caparica (Portugal). E-mail: clodeiro@bioscopegroup.org*
[3] *Department of Inorganic Chemistry, Complutense University of Madrid, Ciudad Universitaria, 28040 Madrid (Spain).*

[†] In loving memory of Professor José A. Campo Santillana

Supporting information to DOI 10.1007/s12274-****-****-* (automatically inserted by the publisher)

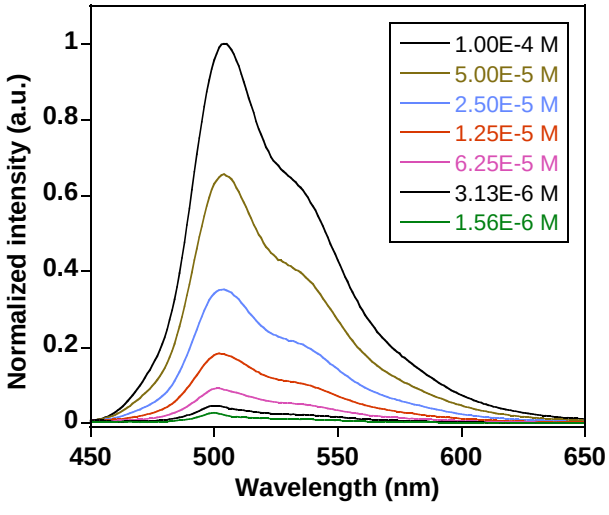

Figure S1 Normalized emission spectrum of **2** in THF solution at selected concentrations.

Address correspondence to Cristián Cuerva, c.alaiz@fct.unl.pt; Carlos Lodeiro, cle@fct.unl.pt

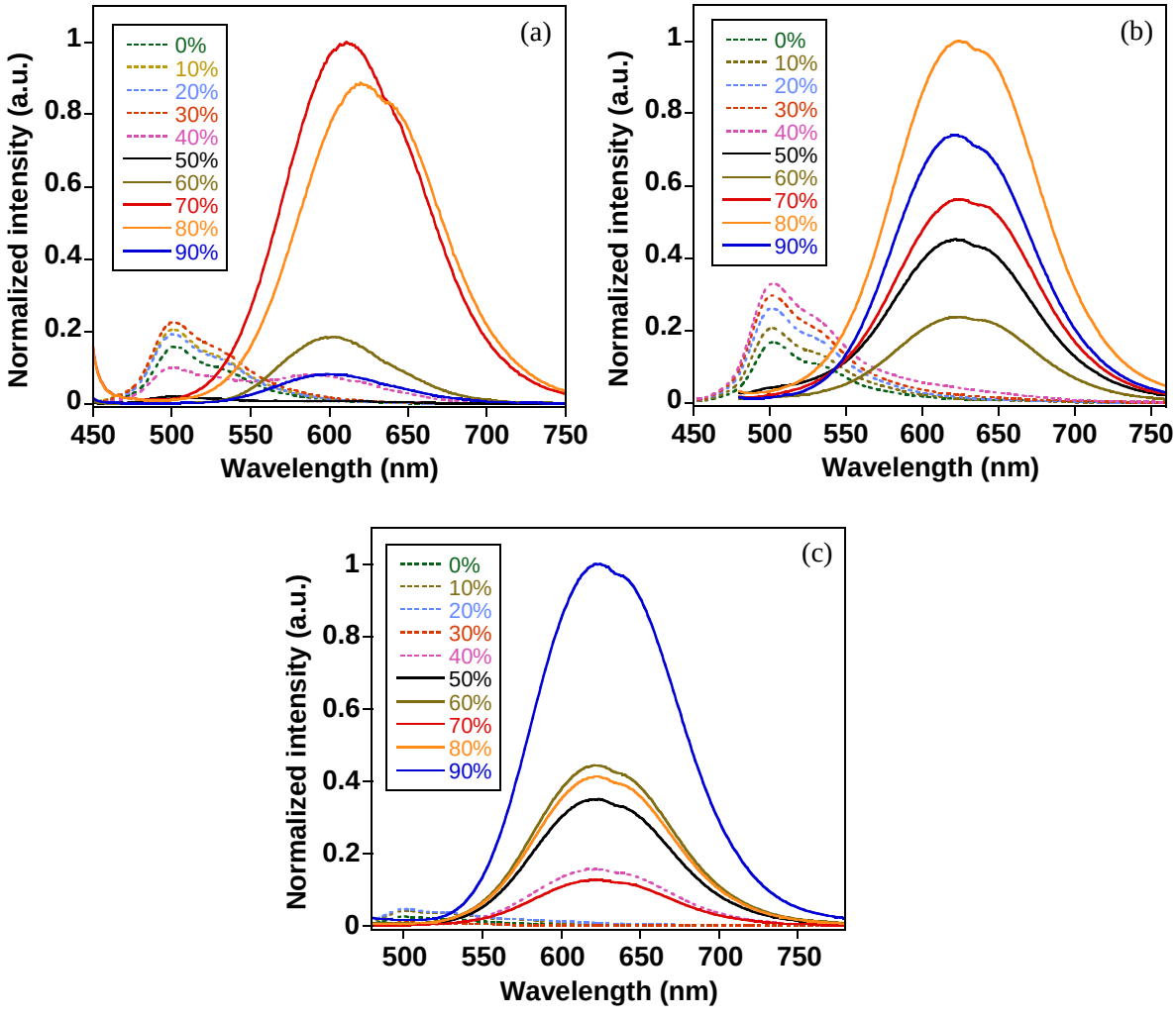

Figure S2 Normalized emission spectra for compounds (a) **1**, (b) **3** and (c) **6**, in the THF/water mixtures as a function of the water fraction f_w.

Table S1 Average hydrodynamic diameter and polydispersity index (PDI) of the Pt(II) aggregates in the THF/water mixtures.

Comp.[a]	f_w (%)	Average diameter ± SD / nm	PDI ± SD
1	80	185.6 ± 1.7	0.09 ± 0.01
	70	301.7 ± 2.2	0.09 ± 0.03
2	80	290.7 ± 2.6	0.20 ± 0.01
	70	455.9 ± 5.3	0.08 ± 0.06
	60	718.1 ± 3.0	0.07 ± 0.04
	50	1182.7 ± 39.4	0.2 ± 0.1
3	80	1332.0 ± 53.5	0.14 ± 0.05
5	90	130.3 ± 1.7	0.14 ± 0.01
	80	143.9 ± 1.0	0.11 ± 0.03
	70	222.8 ± 2.3	0.12 ± 0.02
	60	488.5 ± 4.0	0.13 ± 0.04
	50	1243.0 ± 23.6	0.15 ± 0.01
6	90	232.2 ± 1.4	0.12 ± 0.02

[a] Stable aggregates cannot be obtained from **4**

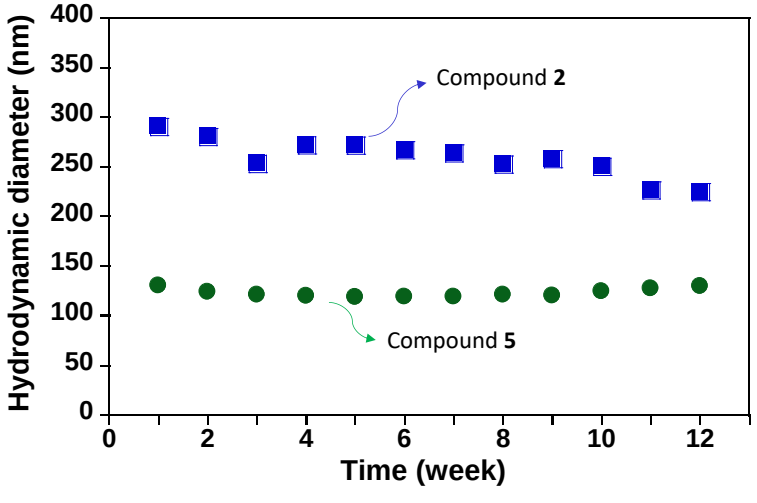

Figure S3 Variations in the average size of the aggregates obtained from **2** (f_w = 80%) and **5** (f_w = 90%) during the first three months.

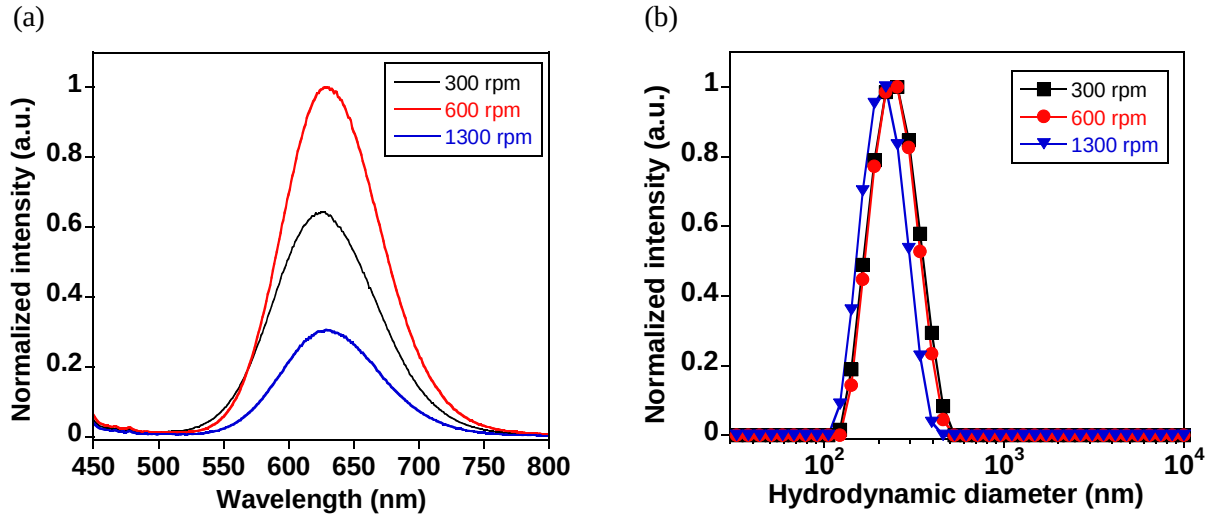

Figure S4 (a) Emission spectra and (b) DLS analysis for the O/W droplets containing the Pt(II) compound **2** obtained at different stirring speeds. All droplets were prepared from THF/water mixtures with f_w = 80 %.

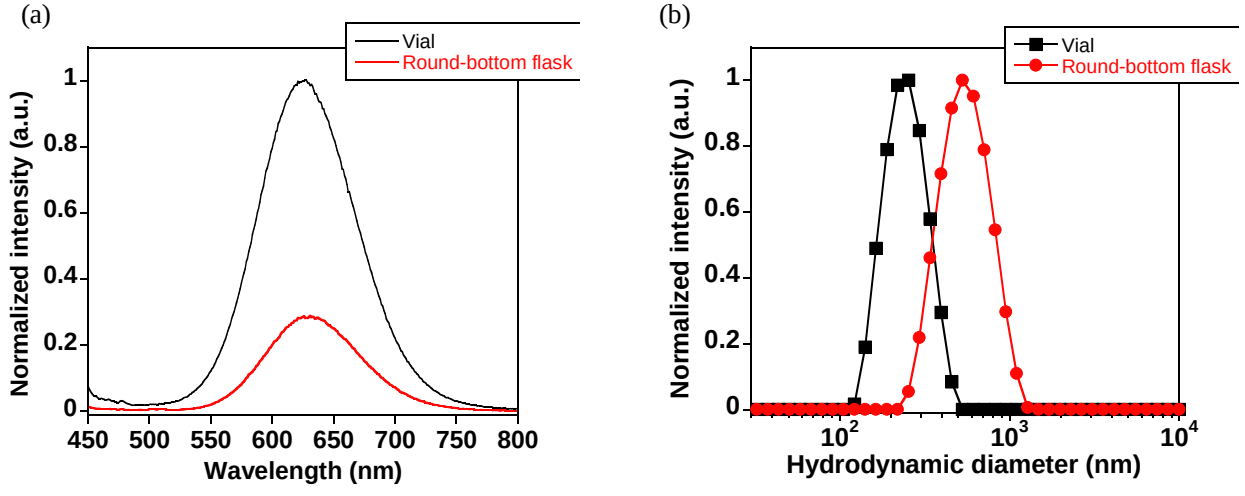

Figure S5 (a) Emission spectra and (b) DLS analysis for the O/W droplets containing the Pt(II) compound **2** obtained by using different reaction vessels. All droplets were prepared from THF/water mixtures with f_w = 80 %.

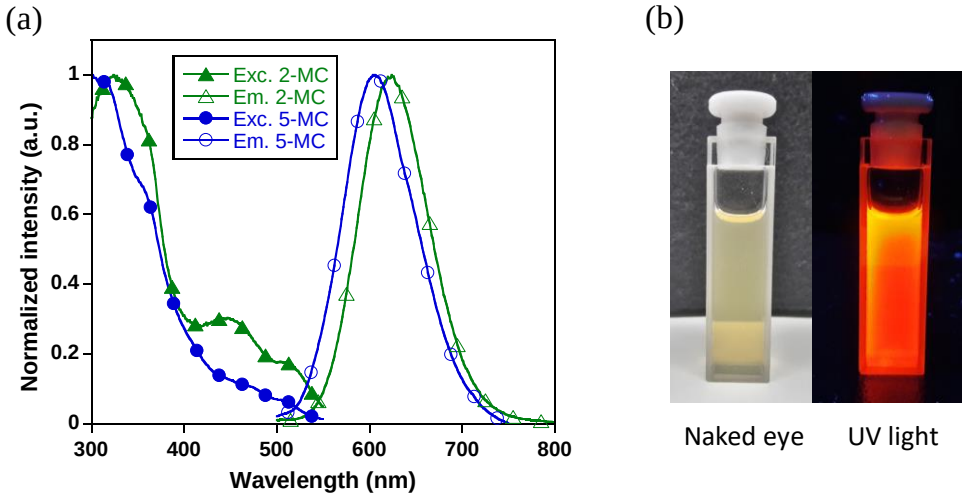

Figure S6 Excitation and emission spectra of the microcrystals obtained from **2** and **5** in water. (b) Images of the colloidal dispersion of microcrystals of **2** taken with the naked eye and under UV light ($\lambda_{exc.}$ = 365 nm).

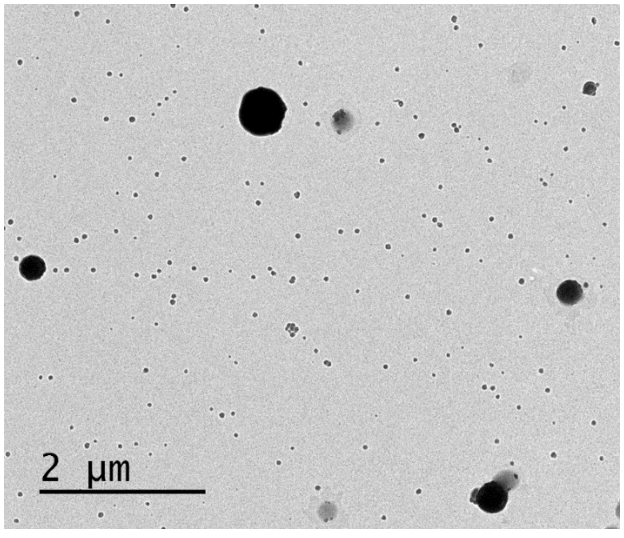

Figure S7 TEM image of nanocrystals obtained from **2** via method 1 with droplet stabilization at 4 ºC, showing the biggest aggregates.

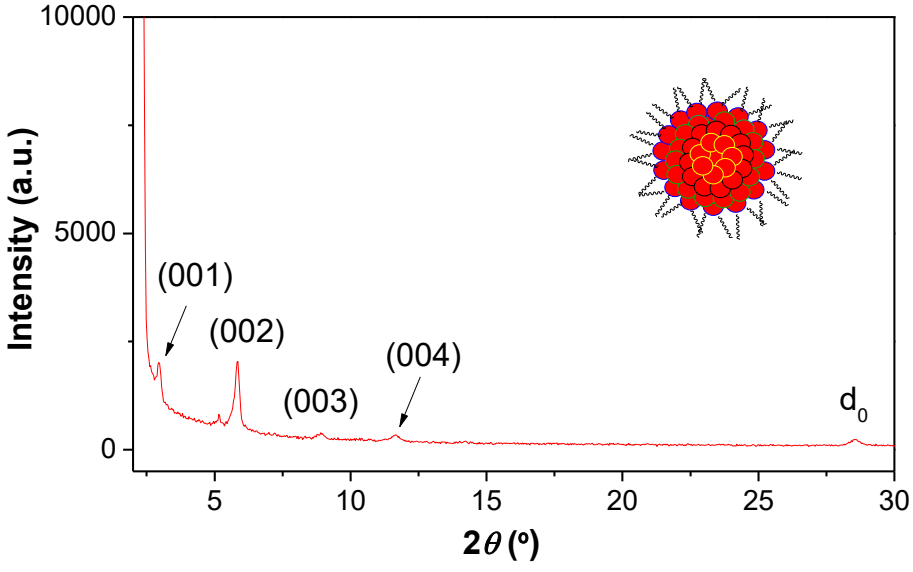

Figure S8 Diffractogram recorded for the microcrystals of **2** prepared via method 1 at 25 ºC. The inset shows a schematic illustration of the lamellar distribution of molecules in the micellar-like microcrystals. Some alkyl chains have been omitted for the sake of clarity.

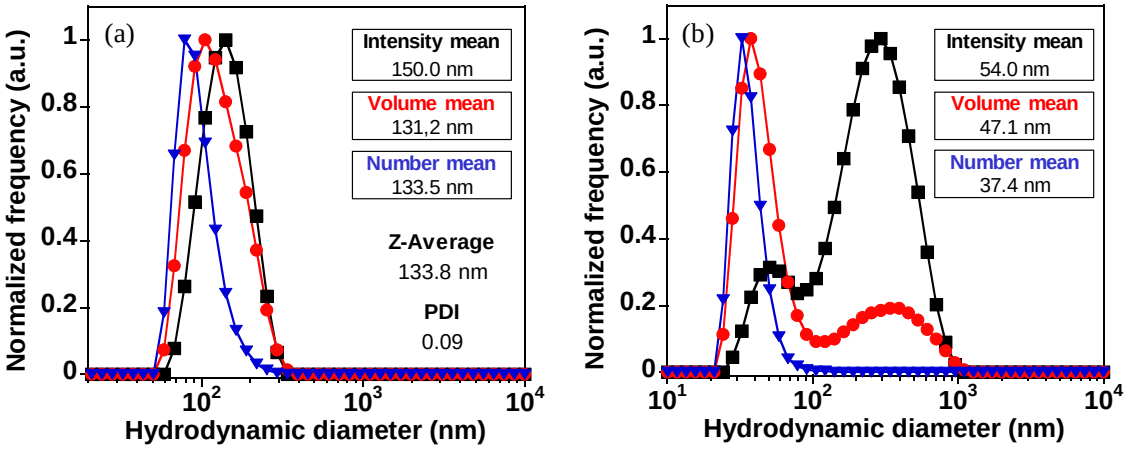

Figure S9 DLS analysis for the micro- and nanocrystals of **5** prepared via method 1 with droplet stabilization at (a) 20ºC, and (b) 4 ºC.

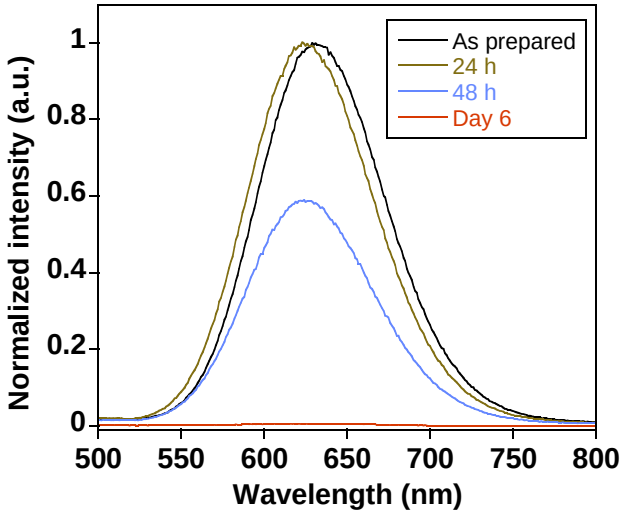

Figure S10 Time-dependent emission spectra of microcrystals obtained from **2** by method 1 at 20 ºC.

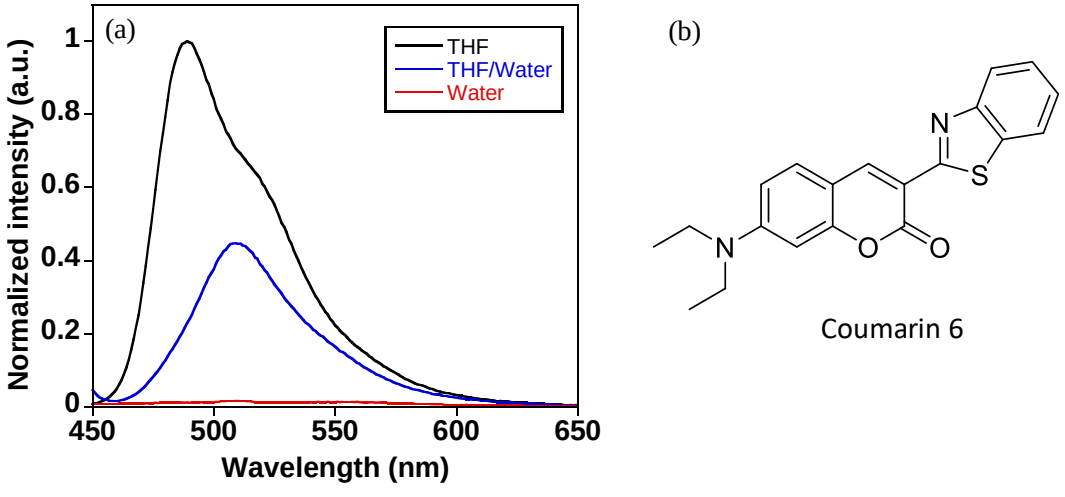

Figure S11 (a) Normalized emission spectra of C6 in pure THF, in THF/Water (f_w = 80), and in pure water. (b) Molecular structure of C6.

Table S2 Encapsulation efficiency and drug-loading capacity for the C6-loaded micro- and nanocrystals obtained from **2** and **5** *via* method 2.

Comp.[a]	Encapsulation efficiency (%)	Drug-loading capacity (%)	Temperature of droplet stabilization (º C)
2	79	16	25
	26	5	4
5	< 5	< 1	25